THE JOURNAL OF
PHYSICAL CHEMISTRY C

Article

pubs.acs.org/JPCC

Enhancing Water Splitting Activity and Chemical Stability of Zinc Oxide Nanowire Photoanodes with Ultrathin Titania Shells

Mingzhao Liu,* Chang-Yong Nam, Charles T. Black, Jovan Kamcev, and Lihua Zhang

Center for Functional Nanomaterials, Brookhaven National Laboratory, Upton, New York 11973, United States

S *Supporting Information*

ABSTRACT: Zinc oxide nanowire photoanodes are chemically stabilized by conformal growth of an ultrathin shell of titania through atomic layer deposition, permitting their stable operation for water splitting in a strongly alkaline solution. Because of the passivation of zinc oxide surface charge traps by titania coating, core/shell nanowire arrays supply a photocurrent density of 0.5 mA/cm^2 under simulated AM1.5G sunlight at the thermodynamic oxygen evolving potential, demonstrating 25% higher photoelectrochemical water splitting activity compared to as-grown zinc oxide wires. By thermally annealing the zinc oxide wire arrays prior to surface passivation, we further increase the photocurrent density to 0.7 mA/cm^2—the highest reported value for doped or undoped zinc oxide photoanodes studied under similar simulated sunlight. Photoexcitations at energies above the zinc oxide band gap are converted with efficiency greater than 80%. Photoluminescence measurements of the best-performing nanowire arrays are consistent with improved water splitting activity from removal of deep trap states.

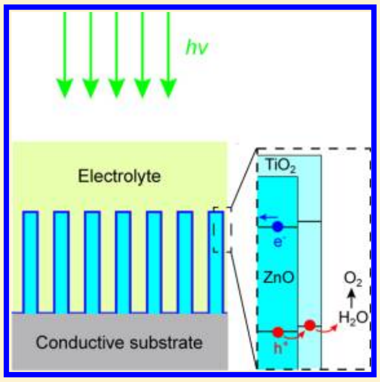

INTRODUCTION

Photoelectrochemical (PEC) water splitting, also known as artificial photosynthesis, has long been thought to be promising for capture and high-capacity storage of solar energy.[1,2] The heart of a typical PEC cell is the semiconductor photoelectrode, in which electron−hole pairs are generated upon light absorption. Following charge carrier separation, electrons reduce water to hydrogen while holes oxidize water to oxygen. The ideal candidate semiconductor electrode is chemically robust against the harsh conditions for water oxidation/reduction and has an electronic band gap small enough to maximize solar light absorption while still providing sufficient energy to drive the water splitting reaction ($2H_2O \rightarrow 2H_2 + O_2$, $V° = 1.23$ V). The semiconductor must also possess suitable electrical conductivity to facilitate charge carrier separation with minimal ohmic loss. Finally, the material must have active reaction centers for charge transfer across the interface to the electrolyte due to the significant overpotential from the four-electron water oxidation half-reaction.[3−5] Despite decades of effort by numerous groups, a material fully satisfying these requirements is yet to be found.[6]

There remains a long-standing significant research interest in PEC water splitting using zinc oxide (ZnO)-based materials.[7−9] Pure ZnO is a wide band gap semiconductor with excellent electronic properties. Naturally doped as n-type due to the presence of donor defects,[10,11] ZnO is a significantly better conductor of both electrons[12,13] and holes[14,15] compared to rutile TiO_2 (a model material for PEC water splitting). Although its wide band gap of 3.37 eV (368 nm) limits the amount of solar light absorption, ZnO can be alloyed with other semiconductors of similar lattice structure, such as GaN or InN, to significantly reduce the band gap.[8,16−18] In addition, ZnO readily forms nanostructures with large surface-to-volume ratios, which enjoy great advantage in PEC water splitting for efficient delivery of photogenerated carriers.[19−21] Despite these excellent properties, ZnO-based photoanodes do not support reliable and efficient PEC water splitting due to several material limitations.[7−9,18] Most notably, ZnO suffers from photocorrosion in aqueous solution under ultraviolet illumination, a common problem for many other candidate materials for water splitting.[22,23] The degradation of ZnO becomes more serious in higher pH solutions, even in the dark.[24] However, an alkaline solution is generally preferred for water splitting photoanodes as the environment provides adequate OH$^-$ ions adsorbed over the electrode surface to receive the photogenerated holes.[25,26]

In this report, we demonstrate that conformal coating of an ultrathin (∼1 nm) titania (TiO_2) shell over a ZnO nanowire array allows it to operate stably as a water splitting photoanode in a strongly alkaline solution—a first for any ZnO-based photoanode.[23] Considering that a water splitting photoanode is typically a minority carrier device,[2] the ultrathin shell is particularly desirable because it minimizes the path for minority carrier diffusion. Similar ZnO/TiO_2 core/shell nanostructures were previously synthesized and studied as electron acceptors (instead of light absorbers) for hybrid solar cells and dye-sensitized solar cells, in which a thicker (≥5 nm) TiO_2 shell improves carrier separation efficiency and suppresses carrier recombination for enhanced device performance.[27,28] In our application, however, the much thinner (1 nm) TiO_2 shell already results in notable enhancement to PEC water splitting

Received: April 23, 2013
Revised: June 5, 2013
Published: June 10, 2013

dx.doi.org/10.1021/jp404032p | *J. Phys. Chem. C* 2013, 117, 13396−13402

efficiency, mainly through passivation of surface states that trap the highly energetic photoholes in the ZnO valence band.[29−31] By combining with further removal of trap states using oxygen plasma treatment and oxidative thermal annealing, we obtain the highest-to-date quantum yield for PEC water splitting using a ZnO-based photoanode.

■ EXPERIMENTAL SECTION

Synthesis of ZnO/TiO$_2$ Core/Shell Nanowire Array. The ZnO nanowire array is grown over an indium tin oxide (ITO) glass substrate using a seed-mediated hydrothermal method that was reported previously.[19,20] To deposit the ZnO seed, an ethanol solution of zinc acetate is drop-cast over the growth substrate, which is then baked at 325 °C for 20 min in air. The seeded substrate is then placed in the growth solution, an aqueous solution of zinc nitrate and hexamethylenetetramine that is heated to 90 °C, for 120 min. After the growth, the nanowire array is thoroughly washed with deionized water and dried in a stream of nitrogen (N_2). The TiO$_2$ shell is coated over the ZnO nanowire array in a Cambridge Nanotech Savannah S100 atomic layer deposition (ALD) system, using titanium isopropoxide and water as precursors. The deposition is carried out at 250 °C for 100 cycles (nominal deposition rate 0.01 nm/cycle), under 300 mTorr of nitrogen carrier gas flowing at 20 sccm. Prior to the TiO$_2$ coating, various processing techniques, including thermal annealing and oxygen plasma cleaning, are applied to the as-grown ZnO nanowire arrays. In Scheme 1, we summarize processing methods and corresponding samples subjected to our investigation. The morphology and compositions of the nanowires are characterized using a Hitachi S-4800 scanning electron microscope and a JEOL JEM2100F transmission electron microscope.

Scheme 1. As-Grown ZnO Nanowire Arrays (Sample I) Are Treated by Various Means To Produce Samples II−IV, Which Are All Coated with an Ultrathin TiO$_2$ Layer by ALD

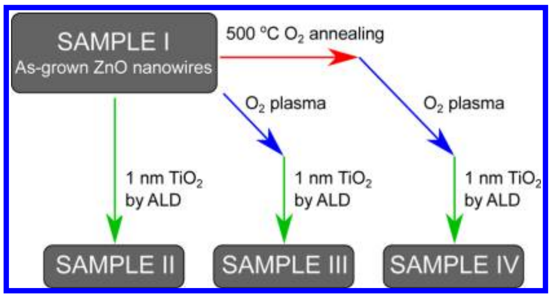

Photoluminescence Measurements. Photoluminescence spectra of the nanowire arrays are measured in an ISS PC1/K2 spectrofluorometer that uses a xenon lamp for optical excitation and a photon multiplier tube for PL detection. The excitation wavelength is set to 280 nm by a monochromator. The PL emission is collected by a second monochromator at the normal direction to the excitation beam. A 320 nm long-pass filter is inserted between the sample and the second monochromator to remove the scattered excitation light.

Electrochemistry and Photoelectrochemistry Measurements. The measurements are performed on a measurement station equipped with a potentiostat (VersaStat, PAR), a custom-built three-electrode quartz-windowed photoelectrochemical cell, and a 150 W solar simulator with AM 1.5G filter (Newport). In the photoelectrochemical cell, we use a 0.1 M KOH solution as an electrolyte, the nanowire array substrate as a working electrode (active/uniform illumination area of 1.0 cm^2), an Ag/AgCl/3 M KCl reference electrode (0.210 V_{NHE}), and a platinum wire counter electrode. The incident light power is calibrated by a calibrated quartz-windowed Si solar cell (Newport) and a spectrometer calibrated for an absolute irradiance measurement (Ocean Optics). For the incident photon-to-current efficiency (IPCE) measurement, we use a 300 W xenon arc lamp and a grating monochromator equipped with band-pass filters for removing higher order diffractions. The light power for each wavelength is measured by an optical power meter (Newport 1918-C) and a UV-enhanced Si photodiode sensor.

■ RESULTS AND DISCUSSION

The as-grown ZnO nanowires have an average diameter of 40 nm and average length of 0.55 μm (Figure 1a), with a packing density of ~2.2 × 10^{10} cm^{-2} (Figure S1 in the Supporting Information) and a single crystalline wurtzite structure with *c*-axis growth direction (Figure 1b). Because of their high aspect ratio and density, the nanowire arrays provide ~15 times more surface area than the planar substrate. The steady-state photoluminescence (PL) spectra of as-grown nanowire arrays show weak band gap emission near 3.3 eV (376 nm), accompanied by a much stronger deep-level emission at ~2.2 eV (560 nm) (Figure 1d) that is generally associated with deep hole traps due to oxygen vacancies with energies ~1 eV above the valence band edge.[21,31] The deep level emission is significantly suppressed after the ZnO nanowire arrays are coated with a nominal 1 nm thick TiO$_2$ shell using atomic layer deposition (ALD) at 250 °C.[27] This core/shell nanostructure shows stronger band gap emission and reduces deep-level emission by nearly 90% (based on the change in integrated PL intensity) compared to an uncoated ZnO nanowire array (Figure 1c), consistent with passivation of bare ZnO surface states. Heat experienced by the nanowires during ALD process (250 °C), however, does not remove the deep levels in significant number (Figure S2).[19] The ZnO/TiO$_2$ core/shell structure is confirmed using energy-dispersive X-ray spectroscopy (EDX) performed in a transmission electron microscope (TEM), as the EDX line scan across an individual nanowire diameter shows a significantly higher fraction of Ti near the edge (Figure 1d). On the basis of the EDX measurement, we estimate the actual thickness T of the TiO$_2$ shell to be 0.9 nm, from the measured Ti/Zn atomic ratio ($N_{Ti}/N_{Zn} = 0.03 \pm 0.003$) through the nanowire center using the relation $N_{Ti}/N_{Zn} = (2V_{m,ZnO}T)/(V_{m,TiO_2}D)$, where $D = 40$ nm is the diameter of the ZnO nanowire and $V_{m,ZnO} = 14.5$ cm^3/mol and $V_{m,TiO_2} = 20.5$ cm^3/mol are the molar volumes of ZnO and TiO$_2$, respectively.

Linear current density−potential (j−E) sweeps (Figure 2a) are performed for the as-grown ZnO nanowire array (sample I), in the dark (black) and under simulated 1 sun (AM1.5G) illumination conditions (red). We measure negligible anodic dark current until applying ~0.6 V overpotential vs $E°(O_2|H_2O)$, the thermodynamic potential for oxygen evolving (dashed vertical line, Figure 2a). Here, we deduce $E°(O_2|H_2O)$ from the Nernst relation, $E°(O_2|H_2O) = (1.23−0.05917$ pH) $V_{NHE} = 0.46$ V_{NHE}, for pH = 13, which is 0.25 V vs the AgCl/Ag reference electrode (0.210 V_{NHE}). The illuminated cell produces significant anodic photocurrent with an onset potential at −0.55 $V_{AgCl/Ag}$, which roughly represents the flat

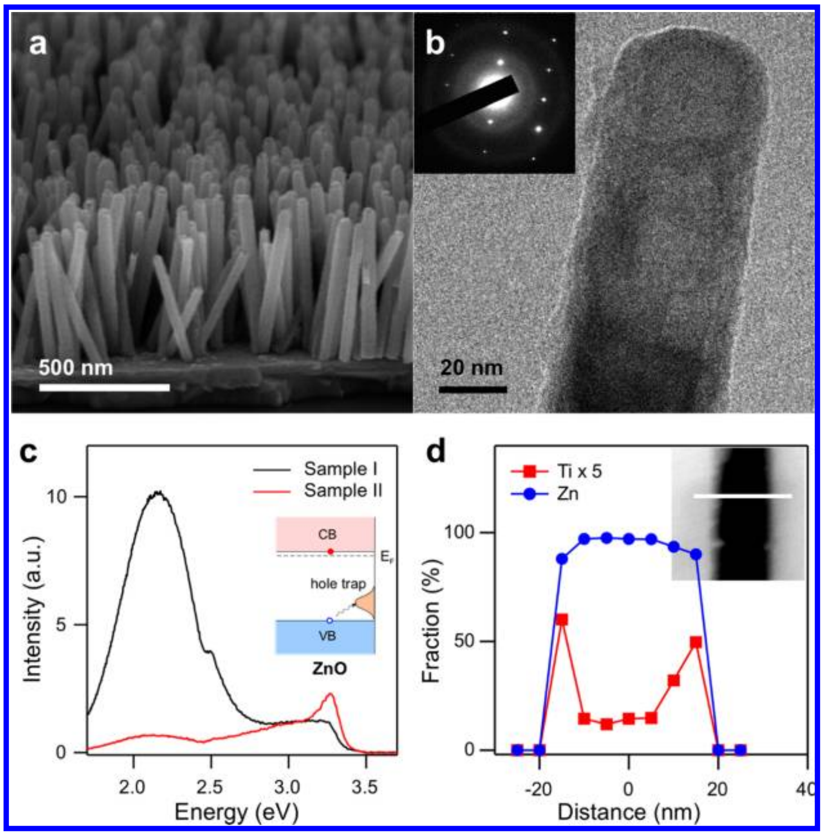

Figure 1. (a) SEM image of a ZnO nanowire array grown on an ITO substrate. (b) TEM image of a ZnO nanowire. Inset: selective area electron diffraction (SAED) pattern of the nanowire. (c) PL spectra of the ZnO nanowire array (sample I, black line) and the ZnO/TiO_2 core/shell nanowire array (sample II, red line). Inset: schematic energy diagram of the ZnO nanowire showing location of the deep hole traps. CB, VB, and E_F are the conduction band edge, valence band edge, and ZnO Fermi level, respectively. (d) EDX elemental line scans of a ZnO/TiO_2 core/shell nanowire (shown in the inset). Oxygen is excluded from the elemental scan.

band potential (E_{fb}) of the system. The anodic photocurrent onset at 0.8 V negative of $E°(O_2|H_2O)$ implies that the PEC system is capable of harvesting solar energy through water splitting. Higher applied voltage leads to further band bending at the ZnO/electrolyte interface, improved charge carrier separation efficiency, and consequently higher photocurrent. At zero overpotential vs $E°(O_2|H_2O)$, the photocurrent output of the as-grown ZnO nanowire array reaches 0.40 mA/cm^2, which is among the highest reported photocurrents for a ZnO-based PEC water splitting cell (Figure 2a).[7,9] The alkaline electrolyte (0.1 M KOH) plays a major role in the measured high performance because it supplies a large OH^- concentration supporting the anodic reaction, $4OH^- + 4h^+ \rightarrow O_2 + 2H_2O$. Reports from similar ZnO nanowire arrays show ~20 times less photocurrent (0.02 mA/cm^2) in a pH neutral electrolyte, under otherwise identical conditions.[7] The PEC water splitting energy conversion efficiency (η) of the as-grown ZnO nanowire array reaches 0.09% at −0.1 $V_{AgCl/Ag}$, when calculated by the following relation:

$$\eta = j_p \frac{E°(O_2|H_2O) - E}{I_0} \times 100\% \qquad (1)$$

where j_p is the photocurrent density, $(E°(O_2|H_2O) - E)$ is the electrode underpotential vs $E°(O_2|H_2O)$, and I_0 = 100 mW/cm^2 is the 1 sun (AM1.5G) incident light power.[32,33] The photocurrent output decreases by ~10% after 1 h of the PEC reaction (blue curve in Figure 2a), with a corresponding decrease in η to 0.08%, due to the slow dissolution of ZnO in the strong alkaline electrolyte.

The PEC water splitting activity and chemical stability of the ZnO nanowire anode are significantly improved after TiO_2 coating and additional processing, which are summarized in Scheme 1. The ZnO/TiO_2 core/shell nanowire array (sample II) shows a qualitatively similar PEC j−E characteristic (red curve in Figure 2b), but with ~25% larger photocurrent (0.5 mA/cm^2) at zero overpotential, compared to as-grown ZnO wires. The maximum energy conversion efficiency improves to 0.10% (at −0.1 $V_{AgCl/Ag}$). Importantly, during the course of 1 h, there is negligible change in the j−E characteristic (blue curve), implying that the chemically inert TiO_2 shell formed by ALD improves ZnO nanowire stability. Measurement over longer duration (≥3 h) does not lead to decay in performance or visible damage to the photoanode. Because the TiO_2 shell is very thin (~1 nm) compared to the ZnO nanowire diameter (~40 nm), the improved performance is not due to additional light absorption in the shell, which was reported for the case of a much thicker TiO_2 coating.[34] Instead, it is consistent with the partial removal of surface trap states as observed in PL.[29,30,35] The ultrathin shell also minimizes the path for the minority carriers (photoholes) to travel from the bulk of ZnO to the photoanode surface.

Further removal of deep trap ZnO surface states enables even more substantial enhancement in the PEC activity of core/shell ZnO/TiO_2 nanowire arrays. Treating as-grown ZnO wire arrays with an oxygen plasma prior to coating with the thin TiO_2 shell (sample III) leads to significantly more intense band edge PL

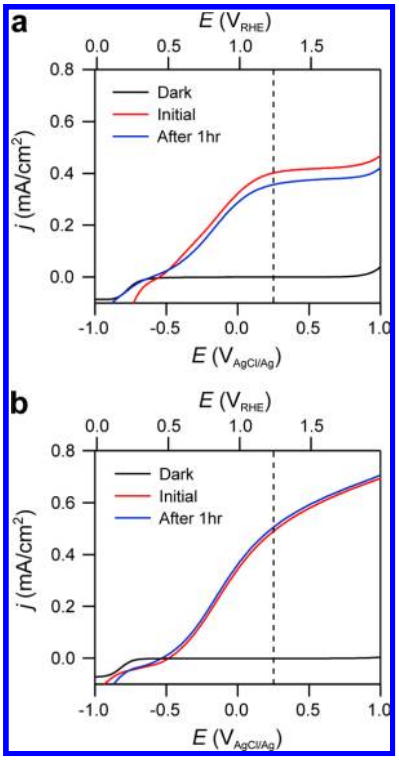

Figure 2. (a) Current density versus potential curves in the dark (black line) and in simulated AM 1.5 illumination for the ZnO nanowire array (sample I) during the initial test (red line) and after 1 h of illumination (blue line). (b) Current density versus potential curves in the dark (black line) and in simulated AM 1.5 illumination for the ZnO/TiO_2 core/shell nanowire array (sample II) during the initial test (red line) and after 1 h of illumination (blue line). In both panels, the thermodynamic potential for oxygen evolution ($E°(O_2|H_2O)$) is indicated by a dashed vertical line, and the top axis is presented as the potential vs RHE (reversible hydrogen electrode). The electrolyte is a 0.1 M KOH aqueous solution with pH = 13.

emission at 3.3 eV (376 nm), which is likely originating from the removal of nonradiative charge traps, i.e., dark states (Figure 3a).[36] Comparing to sample II, PEC cells made from these structures produce a 20% higher photocurrent of 0.61 mA/cm^2 at zero overpotential (Figure 3b) as well as a 30% improvement in $\eta_{max} = 0.13\%$ (at -0.14 $V_{AgCl/Ag}$), demonstrating the positive impact of reducing the deep trap population on the PEC quantum yield. When compared to the as-grown ZnO nanowires (sample I), the photocurrent improves by 52% and the energy conversion efficiency improves by 44%. The increase in energy conversion efficiency results from both increased photocurrent (at zero overpotential) and a higher fill factor (*FF*) of the $j-E$ curve. The higher *FF* reflects reduced charge carrier recombination within the ZnO,[37] consistent with the reduction in charge trap population. Despite these improvements, we measure persistent residual deep level emission in the PL spectrum even after an extended period of plasma cleaning, indicating the presence of trap states in the *bulk* of the ZnO nanowire. Annealing as-grown ZnO nanowire arrays in O_2 at 500 °C before performing the O_2 plasma treatment and growing the TiO_2 shell (sample IV) renders the PL spectrum nearly free of deep level emission (Figure 3a) and further improves its PEC water splitting activity.[38] Such photoanodes produce photocurrent of 0.7 mA/cm^2 at zero overpotential (Figure 3b), with $\eta_{max} \sim 0.17\%$ (at -0.18 $V_{AgCl/Ag}$), representing 75% and 89% respective improvements over the photocurrent and efficiency of the as-grown ZnO nanowires (sample I). The values of zero-overpotential photocurrent and maximum energy conversion efficiency are, to our best knowledge, 75% and 55% higher than any previously reported values for PEC water splitting cells based on a ZnO photoanode.[7−9,18] The stabilities of samples III and IV are similar to sample II, again confirming the effectiveness of the TiO_2 shell in protecting the nanowire photoanodes.

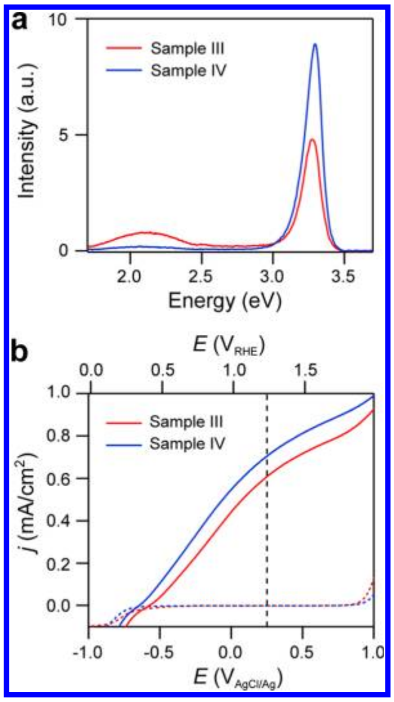

Figure 3. (a) PL spectra of the ZnO/TiO_2 core/shell nanowire array that has the ZnO core plasma cleaned but unannealed (sample III, red line) and the one that has the ZnO core thermally annealed and plasma cleaned (sample IV, blue line). (b) Current density versus potential curves in simulated AM 1.5 illumination for sample III (red line) and sample IV (blue line). The dark $j-E$ curves for each sample are shown as dotted lines of corresponding color. The thermodynamic potential for oxygen evolution ($E°(O_2|H_2O)$) is indicated by a dashed vertical line and the top axis is presented as the potential vs RHE. The electrolyte is a 0.1 M KOH aqueous solution with pH = 13.

We understand further details of the anodic PEC reaction by measuring the incident photon-to-current efficiency (IPCE), defined as the ratio of the number of collected photogenerated electrons to the number of incident photons. The measurements are performed at zero overpotential for incident photon energies between 2.6−4 eV (477−310 nm). Surface passivated ZnO/TiO_2 core/shell wires (sample III) achieve an IPCE of >60% for 3.4 eV (365 nm) incident photons (Figure 4), with little variation at higher energies. Because ZnO has a direct band gap with strong optical absorption at energies larger than the band gap, the constant IPCE over this range likely indicates near complete photon absorption, with quantum efficiency limited by inefficiencies in charge transport, remaining charge traps, and subsequent electron−hole recombination. For lower incident photon energies, the IPCE drops to zero, consistent with a ZnO band gap of ~3.3 eV (376 nm). Core/shell ZnO/TiO_2 nanowires thermally annealed in oxygen before surface passivation (sample IV) achieve an IPCE of ≥80% for energies above 3.4 eV (365 nm) and have a qualitatively identical spectral dependence to unannealed core/shell wires with only surface passivation (sample III). By integrating the IPCE

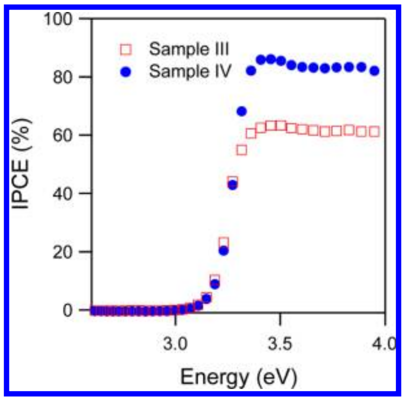

Figure 4. Incident photon-to-current efficiency (IPCE) as a function of excitation energy, the ZnO/TiO$_2$ core/shell nanowire array that has the ZnO core plasma cleaned but unannealed (sample III, open squares), and the one that has the ZnO core thermally annealed and plasma cleaned (sample IV, solid dots). The measurements are performed in a 0.1 M KOH aqueous solution with pH = 13, at the thermodynamic potential for oxygen evolution ($E°(O_2|H_2O)$).

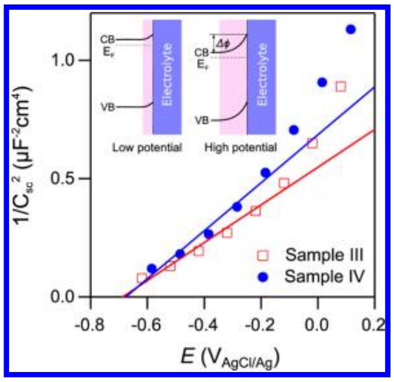

Figure 5. Mott−Schottky plots for sample III (ZnO core unannealed, open squares) and sample IV (ZnO core annealed, solid dots). Solid colored lines are corresponding linear fits to the data for $E < -0.1$ V$_{AgCl/Ag}$. Inset: schematic representation of band bending ($\Delta\phi$) at an n-type semiconductor/electrolyte interface for low (left panel) and high (right panel) electrode potentials. The space charge region, shown in magenta shade, broadens with increasing band bending.

spectra multiplied by the tabulated reference AM1.5 spectrum, the samples' expected photocurrent densities under true AM1.5G sunlight are 0.58 mA/cm^2 for sample III and 0.73 mA/cm^2 for sample IV, which agree well with their experimental values. The improved IPCE after thermal annealing is consistent with removal of deep hole traps and improved charge transport. Although the overall energy conversion efficiency η of ZnO is lower than other more extensively studied water splitting materials such as TiO$_2$ (~1%) or Fe$_2$O$_3$ (~0.3%), its quantum efficiency in the UV region is comparable to or better than the highest values reported for these materials (~90% for TiO$_2$ and 40−50% for α-Fe$_2$O$_3$).[32,39]

Internal electronic properties of the nanowires, including the flat-band potential (E_{fb}) and charge carrier concentration, are determined by measuring the space-charge (or depletion) capacitance per unit area of interface (C_{sc}) versus the electrode potential, E. The capacitance C_0 is extracted from electrochemical impedance spectroscopy performed in the frequency range 10−10^4 Hz and is normalized by the actual surface area A of the ZnO nanowires to obtain C_{sc} (see Supporting Information). For a planar semiconductor/electrolyte interface, the relationship between capacitance and electrode potential varies according to the Mott−Schottky equation:

$$\frac{1}{C_{sc}^{2}} = \frac{A^{2}}{C_{0}^{2}} = \frac{2}{e\varepsilon\varepsilon_{0}N_{D}}\left(E - E_{fb} - \frac{k_{B}T}{e}\right) \qquad (2)$$

where e is the magnitude of the elementary charge, ε the semiconductor dielectric constant (~10 for ZnO),[40] ε_0 the vacuum permittivity, N_D the semiconductor carrier density, k_BT the thermal energy, and $(E - E_{fb}) = \Delta\phi$ is the magnitude of band bending at the semiconductor/electrolyte interface (Figure 5).[41] Measurements of ZnO/TiO$_2$ wires both without (sample III) and with thermal annealing in O$_2$ (sample IV) show a linear relationship between $1/C_{sc}^2$ and E for low potential (<−0.1 V$_{AgCl/Ag}$) which increases superlinearly at higher potential when the depletion width approaches the nanowire radius (Figure 5, inset).[40] A positive slope to these curves indicates that nanowires are doped n-type. Fitting the linear part of the data ($E < -0.1$ V$_{AgCl/Ag}$) to eq 2 permits estimation of both E_{fb} and N_D. Unannealed, surface-passivated core/shell wires (sample III) have E_{fb} at (−0.68 ± 0.03) V$_{AgCl/Ag}$ and N_D as high as 1.8 × 10^{19} cm^{-3}. Thermal annealing (sample IV) leaves E_{fb} unchanged at (−0.68 ± 0.03) V$_{AgCl/Ag}$ and similar N_D ~1.4 × 10^{19} cm^{-3}. The flat band potential E_{fb} is very close to the photocurrent onset for thermally annealed wires (sample IV) (−0.65 V$_{AgCl/Ag}$) but 0.1 V more negative than that of the unannealed wires (sample III) (−0.55 V$_{AgCl/Ag}$), meaning that charge carrier separation efficiency in the absence of band bending (i.e., near E_{fb}) is improved by thermal annealing. This is consistent with thermal annealing removing bulk defects and consequently increasing carrier diffusion length. We note that oxidative thermal annealing has little effect on the charge carrier density, despite eliminating deep traps related to oxygen vacancies. This observation is consistent with density functional theory work by Van de Walle et al., which suggests that the deep donors such as oxygen vacancies are unlikely to contribute to the n-type conductivity of ZnO.[10,42]

■ CONCLUSIONS

PEC water splitting performance of vertically oriented ZnO nanowire arrays is significantly improved by conformally coating of an ultrathin TiO$_2$ shell and systematically passivating both the surface and bulk of the material. The ultrathin shell chemically protects the ZnO nanowires and allows a first demonstration of ZnO-based PEC water splitting in a strongly alkaline environment, which is essential for efficient mass transport near the photoanode and high PEC activity. The TiO$_2$ shell also passivates ZnO nanowire array surface states through partially removal of the deep hole traps, without affecting the minority carrier diffusion due to its almost negligible thickness, consequently increasing the photocurrent output. Combined oxygen plasma treatment and thermal annealing of the ZnO wire core prior to growth of the TiO$_2$ shell further eliminates the bulk-originating defect states, resulting in the highest reported photocurrent density and energy conversion efficiency for a ZnO-based PEC water splitting system. We attribute the exceptional performance to improved charge transport due to removal of trap states. Presently, the development of narrow band gap photocatalysts is frequently plagued by the poor surface properties and their tendency toward photocorrosion. The demonstrated strategies of utilizing a core/shell structure to protect and passivate the photoanode surface and removing bulk defects through thermal processing can be readily generalized to these novel materials, thus opening a new avenue for development of higher performing and more stable materials for PEC water splitting.

■ ASSOCIATED CONTENT

Ⓢ Supporting Information

Top-view SEM image of the nanowire array; photoluminescence spectra of ZnO and ZnO/TiO_2 core/shell nanowire arrays; energy dispersive X-ray spectra of ZnO/TiO_2 core/shell nanowire; details of electrochemical impedance spectroscopy measurements. This material is available free of charge via the Internet at http://pubs.acs.org.

■ AUTHOR INFORMATION

Corresponding Author

*E-mail: mzliu@bnl.gov (M.L.).

Notes

The authors declare no competing financial interest.

■ ACKNOWLEDGMENTS

Research is carried out at the Center for Functional Nanomaterials, Brookhaven National Laboratory, which is supported by the U.S. Department of Energy, Office of Basic Energy Sciences, under Contract DE-AC02-98CH10886.

■ REFERENCES

(1) Fujishima, A.; Honda, K. Electrochemical photolysis of water at a semiconductor electrode. *Nature* **1972**, *238*, 37−38.

(2) Nozik, A. J. Photoelectrochemistry - applications to solar-energy conversion. *Annu. Rev. Phys. Chem.* **1978**, *29*, 189−222.

(3) Shen, X. A.; Small, Y. A.; Wang, J.; Allen, P. B.; Fernandez-Serra, M. V.; Hybertsen, M. S.; Muckerman, J. T. Photocatalytic water oxidation at the GaN ($10\bar{1}0$)-water interface. *J. Phys. Chem. C* **2010**, *114*, 13695−13704.

(4) Kanan, M. W.; Nocera, D. G. In situ formation of an oxygen-evolving catalyst in neutral water containing phosphate and Co^{2+}. *Science* **2008**, *321*, 1072−1075.

(5) Seabold, J. A.; Choi, K. S. Efficient and stable photo-oxidation of water by a bismuth vanadate photoanode coupled with an iron oxyhydroxide oxygen evolution catalyst. *J. Am. Chem. Soc.* **2012**, *134*, 2186−2192.

(6) Walter, M. G.; Warren, E. L.; McKone, J. R.; Boettcher, S. W.; Mi, Q. X.; Santori, E. A.; Lewis, N. S. Solar water splitting cells. *Chem. Rev.* **2010**, *110*, 6446−6473.

(7) Yang, X. Y.; Wolcott, A.; Wang, G. M.; Sobo, A.; Fitzmorris, R. C.; Qian, F.; Zhang, J. Z.; Li, Y. Nitrogen-doped ZnO nanowire arrays for photoelectrochemical water splitting. *Nano Lett.* **2009**, *9*, 2331−2336.

(8) Ahn, K. S.; Yan, Y.; Shet, S.; Deutsch, T.; Turner, J.; Al-Jassim, M. Enhanced photoelectrochemical responses of ZnO films through Ga and N codoping. *Appl. Phys. Lett.* **2007**, *91*, 231909.

(9) Ahn, K. S.; Yan, Y.; Shet, S.; Jones, K.; Deutsch, T.; Turner, J.; Al-Jassim, M. ZnO nanocoral structures for photoelectrochemical cells. *Appl. Phys. Lett.* **2008**, *93*, 163117.

(10) Janotti, A.; Van de Walle, C. G. , Fundamentals of zinc oxide as a semiconductor. *Rep. Prog. Phys.* **2009**, *72*, 126501.

(11) Hofmann, D. M.; Hofstaetter, A.; Leiter, F.; Zhou, H. J.; Henecker, F.; Meyer, B. K.; Orlinskii, S. B.; Schmidt, J.; Baranov, P. G. Hydrogen: A relevant shallow donor in zinc oxide. *Phys. Rev. Lett.* **2002**, *88*, 045504.

(12) Look, D. C.; Reynolds, D. C.; Sizelove, J. R.; Jones, R. L.; Litton, C. W.; Cantwell, G.; Harsch, W. C. Electrical properties of bulk ZnO. *Solid State Commun.* **1998**, *105*, 399−401.

(13) Breckenridge, R. G.; Hosler, W. R. Electrical properties of titanium dioxide semiconductors. *Phys. Rev.* **1953**, *91*, 793−802.

(14) Look, D. C.; Reynolds, D. C.; Litton, C. W.; Jones, R. L.; Eason, D. B.; Cantwell, G. Characterization of homoepitaxial p-type ZnO grown by molecular beam epitaxy. *Appl. Phys. Lett.* **2002**, *81*, 1830−1832.

(15) van de Krol, R.; Grätzel, M. *Photoelectrochemical Hydrogen Production*; Springer: New York, 2012.

(16) Maeda, K.; Takata, T.; Hara, M.; Saito, N.; Inoue, Y.; Kobayashi, H.; Domen, K. GaN: ZnO solid solution as a photocatalyst for visible-light-driven overall water splitting. *J. Am. Chem. Soc.* **2005**, *127*, 8286−8287.

(17) Maeda, K.; Teramura, K.; Lu, D. L.; Takata, T.; Saito, N.; Inoue, Y.; Domen, K. Photocatalyst releasing hydrogen from water - Enhancing catalytic performance holds promise for hydrogen production by water splitting in sunlight. *Nature* **2006**, *440*, 295−295.

(18) Hashiguchi, H.; Maeda, K.; Abe, R.; Ishikawa, A.; Kubota, J.; Domen, K. Photoresponse of GaN:ZnO electrode on FTO under visible light irradiation. *Bull. Chem. Soc. Jpn.* **2009**, *82*, 401−407.

(19) Greene, L. E.; Law, M.; Goldberger, J.; Kim, F.; Johnson, J. C.; Zhang, Y. F.; Saykally, R. J.; Yang, P. D. Low-temperature wafer-scale production of ZnO nanowire arrays. *Angew. Chem., Int. Ed.* **2003**, *42*, 3031−3034.

(20) Greene, L. E.; Law, M.; Tan, D. H.; Montano, M.; Goldberger, J.; Somorjai, G.; Yang, P. D. General route to vertical ZnO nanowire arrays using textured ZnO seeds. *Nano Lett.* **2005**, *5*, 1231−1236.

(21) Shim, M.; Guyot-Sionnest, P. Organic-capped ZnO nanocrystals: Synthesis and n-type character. *J. Am. Chem. Soc.* **2001**, *123*, 11651−11654.

(22) Gerischer, H. Stability of semiconductor electrodes against photodecomposition. *J. Electroanal. Chem.* **1977**, *82*, 133−143.

(23) Chen, Y. W.; Prange, J. D.; Duhnen, S.; Park, Y.; Gunji, M.; Chidsey, C. E. D.; McIntyre, P. C. Atomic layer-deposited tunnel oxide stabilizes silicon photoanodes for water oxidation. *Nat. Mater.* **2011**, *10*, 539−544.

(24) Frank, S. N.; Bard, A. J. Heterogeneous photocatalytic oxidation of cyanide and sulfite in aqueous-solutions at semiconductor powders. *J. Phys. Chem.* **1977**, *81*, 1484−1488.

(25) Williams, F.; Nozik, A. J. Irreversibilities in mechanism of photoelectrolysis. *Nature* **1978**, *271*, 137−139.

(26) Beermann, N.; Vayssieres, L.; Lindquist, S. E.; Hagfeldt, A. Photoelectrochemical studies of oriented nanorod thin films of hematite. *J. Electrochem. Soc.* **2000**, *147*, 2456−2461.

(27) Law, M.; Greene, L. E.; Radenovic, A.; Kuykendall, T.; Liphardt, J.; Yang, P. D. ZnO-Al_2O_3 and ZnO-TiO_2 core-shell nanowire dye-sensitized solar cells. *J. Phys. Chem. B* **2006**, *110*, 22652−22663.

(28) Greene, L. E.; Law, M.; Yuhas, B. D.; Yang, P. D. ZnO-TiO_2 core-shell nanorod/P3HT solar cells. *J. Phys. Chem. C* **2007**, *111*, 18451−18456.

(29) Le Formal, F.; Tétreault, N.; Cornuz, M.; Moehl, T.; Grätzel, M.; Sivula, K. Passivating surface states on water splitting hematite photoanodes with alumina overlayers. *Chem. Sci.* **2011**, *2*, 737−743.

(30) Hwang, Y. J.; Hahn, C.; Liu, B.; Yang, P. D. Photoelectrochemical properties of TiO_2 nanowire arrays: A study of the dependence on length and atomic layer deposition coating. *ACS Nano* **2012**, *6*, 5060−5069.

(31) Monticone, S.; Tufeu, R.; Kanaev, A. V. Complex nature of the UV and visible fluorescence of colloidal ZnO nanoparticles. *J. Phys. Chem. B* **1998**, *102*, 2854−2862.

(32) Liu, M. Z.; Snapp, N. D.; Park, H. Water photolysis with a cross-linked titanium dioxide nanowire anode. *Chem. Sci.* **2011**, *2*, 80−87.

(33) Chen, Z. B.; Jaramillo, T. F.; Deutsch, T. G.; Kleiman-Shwarsctein, A.; Forman, A. J.; Gaillard, N.; Garland, R.; Takanabe, K.; Heske, C.; Sunkara, M.; McFarland, E. W.; Domen, K.; Miller, E. L.; Turner, J. A.; Dinh, H. N. Accelerating materials development for photoelectrochemical hydrogen production: Standards for methods, definitions, and reporting protocols. *J. Mater. Res.* **2010**, *25*, 3−16.

(34) Fan, J. D.; Zamani, R.; Fabrega, C.; Shavel, A.; Flox, C.; Ibanez, M.; Andreu, T.; Lopez, A. M.; Arbiol, J.; Morante, J. R.; Cabot, A.

Solution-growth and optoelectronic performance of ZnO:Cl/TiO_2 and ZnO:Cl/Zn_xTiO_y/TiO_2 core-shell nanowires with tunable shell thickness. *J. Phys. D: Appl. Phys.* **2012**, *45*, 415301.

(35) Hines, M. A.; Guyot-Sionnest, P. Synthesis and characterization of strongly luminescing ZnS-capped CdSe nanocrystals. *J. Phys. Chem.* **1996**, *100*, 468−471.

(36) Zhao, Q.; Cai, T. C.; Wang, S.; Zhu, R.; Liao, Z. M.; Yu, D. P. Enhanced near-band-edge emission and field emission properties from plasma treated ZnO nanowires. *Appl. Phys. A: Mater. Sci. Process.* **2010**, *100*, 165−170.

(37) Zhang, Y.; Dang, X.-D.; Kim, C.; Nguyen, T.-Q. Effect of charge recombination on the fill factor of small molecule bulk heterojunction solar cells. *Adv. Energy Mater.* **2011**, *1*, 610−617.

(38) Zhao, Q.; Xu, X. Y.; Song, X. F.; Zhang, X. Z.; Yu, D. P.; Li, C. P.; Guo, L. Enhanced field emission from ZnO nanorods via thermal annealing in oxygen. *Appl. Phys. Lett.* **2006**, *88*, 033102.

(39) Sivula, K.; Le Formal, F.; Grätzel, M. Solar water splitting: Progress using hematite (α-Fe_2O_3) photoelectrodes. *ChemSusChem* **2011**, *4*, 432−449.

(40) Mora-Seró, I.; Fabregat-Santiago, F.; Denier, B.; Bisquert, J.; Tena-Zaera, R.; Elias, J.; Lévy-Clément, C. Determination of carrier density of ZnO nanowires by electrochemical techniques. *Appl. Phys. Lett.* **2006**, *89*, 203117.

(41) Bard, A. J.; Faulkner, L. R. *Electrochemical Methods: Fundamentals and Applications*; Wiley: New York, 1980.

(42) Van de Walle, C. G. Hydrogen as a cause of doping in zinc oxide. *Phys. Rev. Lett.* **2000**, *85*, 1012−1015.

Supporting information for "Enhancing water splitting activity and chemical stability of zinc oxide nanowire photoanodes with ultrathin titania shells"

Mingzhao Liu, Chang-Yong Nam, Charles T. Black, Jovan Kamcev,* and *Lihua Zhang*

Center for Functional Nanomaterials, Brookhaven National Laboratory, Upton, New York 11973, USA

*E-mail: mzliu@bnl.gov

The measurement of space-charge region capacitance. The impedance of the electrochemical cell (Z) is measured under dark at a series of electrode potentials, in the frequency (f) range 10 to 10^4 Hz. The area of the working electrode is 1.0 cm^2. Shown in Figure S4 are the measurement results for *Sample IV* at -0.38 $V_{AgCl/Ag}$. To extract the space-charge region capacitance from the experimental impedance, the electrochemical cell is modeled as an equivalent circuit shown in the inset of Figure S4.[1] The current passing through the cell contributes in parallel to faradic process that is represented by the charge transfer resistance R_{ct} and nonfaradic interface charging that is represented by C, the capacitance per unit area of interface. The two current components flow together through the electrolyte solution and the electrical contact to the working electrode, which is represented by a series resistance R_1. The capacitance C includes the space-charge region capacitance (C_{sc}) and the double-layer capacitance (C_{dl}) in series, $1/C = 1/C_{sc} + 1/C_{dl}$.

Since C_{dl} is usually orders of magnitude larger than C_{sc}, the total capacitance C roughly equals to C_{sc}.[2] The total impedance of the equivalent circuit writes

$$Z(\omega) = R_1 + \frac{R_{ct}Z_C}{R_{ct}+Z_C} = R_1 - \frac{iR_{ct}/\omega C_{sc}A}{R_{ct}-i/\omega C_{sc}A} = R_1 - \frac{iR_{ct}/\omega C_{sc}A}{R_{ct}-i/\omega C_{sc}A}, \tag{S1}$$

where $\omega = 2\pi f$ is the angular frequency, A is the area of the interface, and $Z_C = -i/\omega C_{sc}A$ is the capacitor impedance. The real and imaginary parts of the complex impedance are thus,

$$\mathrm{Re}(Z) = R_1 + \frac{R_{ct}}{1+\omega^2 R_{ct}^2 C_{sc}^2 A^2}, \tag{S2}$$

$$\mathrm{Im}(Z) = -\frac{\omega R_{ct}^2 C_{sc} A}{1+\omega^2 R_{ct}^2 C_{sc}^2 A^2}. \tag{S3}$$

The nanowires have mean size of 40 nm in diameter and 550 nm in length, with a packing density of 2.2 x 10^{10} cm^{-2} on the substrate, from which we can calculate a surface area A = 15.2 cm^2 for the 1 cm^2 working electrode. The experimental data shown in Figure S4 is then fit to Eqs. S2 and S3 using the EIS Spectrum Analyser, a freeware for analysis of impedance spectrum.[3] From which we obtain R_1 = 1.51 x 10^2 Ω, R_{ct} = 1.29 x 10^4 Ω, and C_{sc} = 1.94 μF cm^{-2}. The capacitances at other potentials are obtained following the same procedure and are presented in Figure 5.

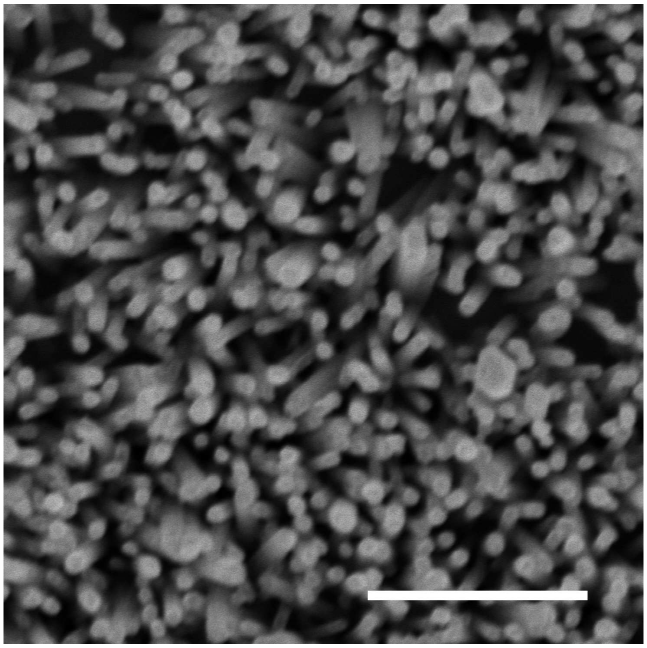

Figure S1. SEM image of a ZnO nanowire array grown on ITO substrate, top view. Scale bar = 500 nm.

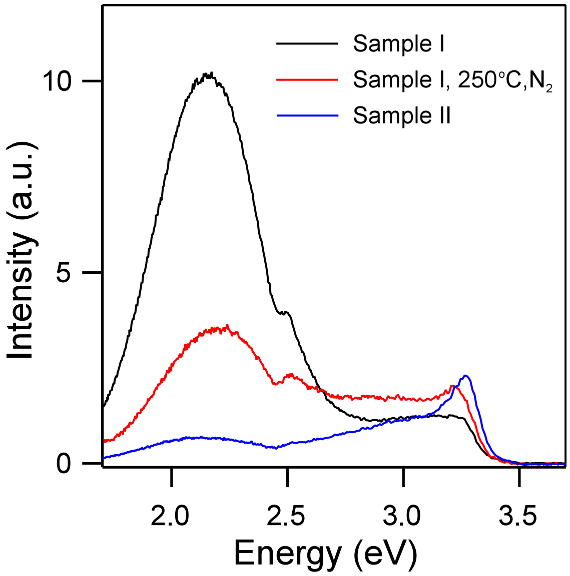

Figure S2. Photoluminescence spectra of as-grown ZnO nanowire array (*Sample I,* black line), ZnO/TiO_2 core/shell nanowire array (*Sample II,* blue line), and a control sample (red line) obtained by annealing a *Sample I* in N_2 at 250°C for 30 min, same duration as the time required for TiO_2 atomic layer deposition (also at 250°C). For the control sample the deep-level emission is reduced compared to *Sample I*, but remains very significant. The deep-level emission is much lower for the ZnO/TiO_2 core/shell nanowire array (*Sample II*), reflecting the passivation of ZnO surface states by ALD TiO_2 coating.

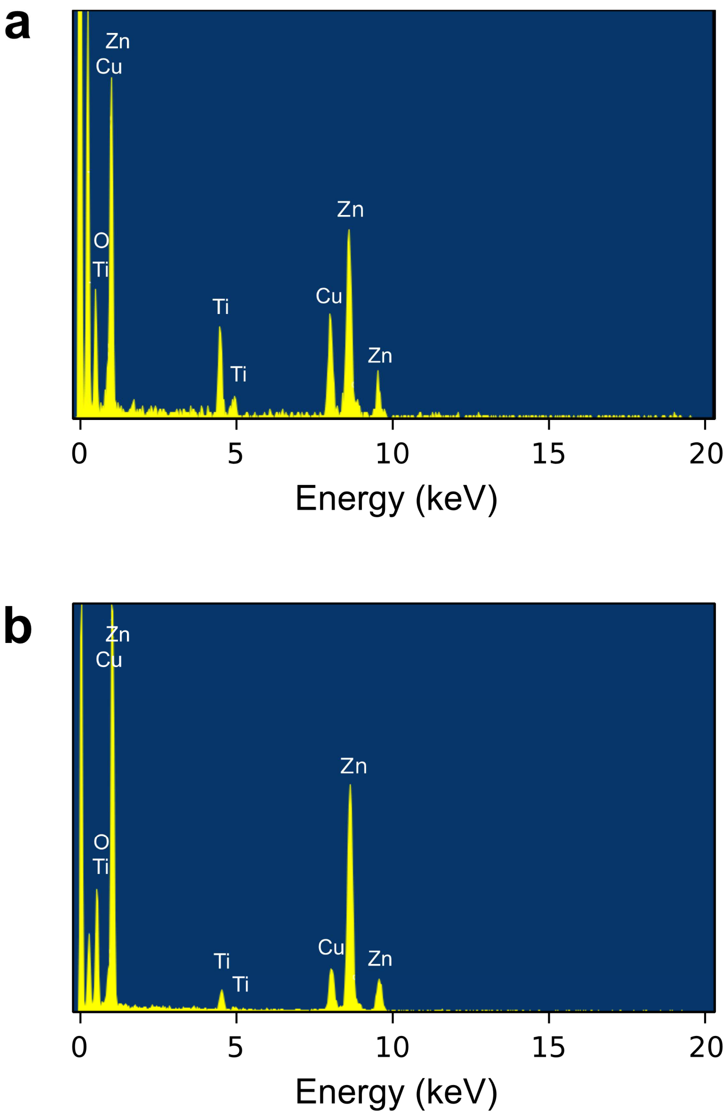

Figure S3. Energy dispersive X-ray (EDX) spectra of the ZnO/TiO_2 core/shell nanowire shown in Figure 1(c), taken near its edge (a) and at its center (b).

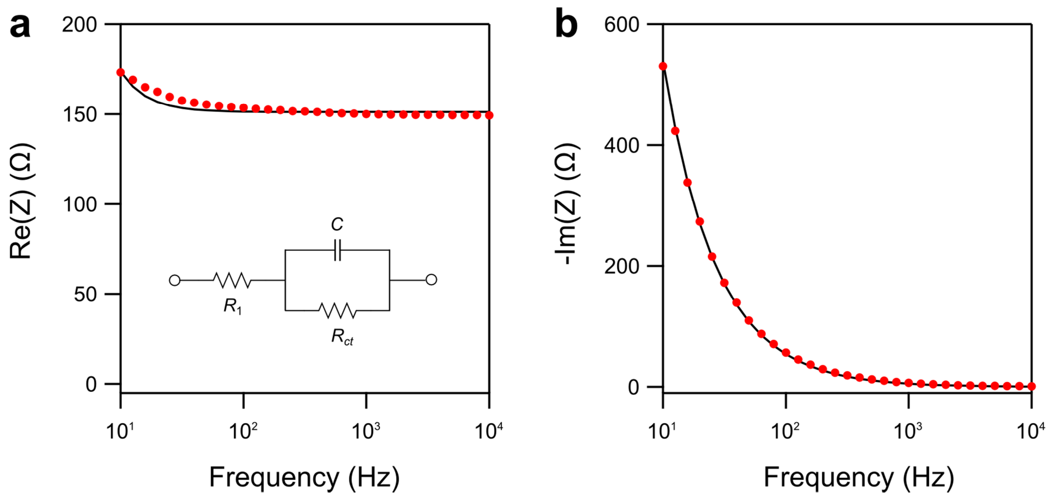

Figure S4. (a) The real and (b) imaginary parts of the cell impedance. The red dots are experimental results taken at -0.38 $V_{AgCl/Ag}$ for *Sample IV* and the solid lines are numerical fitting using the equivalent circuit shown in the inset.

REFERENCES

[1] Bard, A. J.; Faulkner, L. R., *Electrochemical methods: fundamentals and applications*. Wiley: New York, 1980.

[2] Grätzel, M., Photoelectrochemical cells. *Nature* **2001**, 414, 338-344.

[3] Bondarenko, A. S.; Ragoisha, G. A. *EIS Spectrum Analyser*, http://www.abc.chemistry.bsu.by/vi/analyser/.